



AIAA 96-0078

**WAKE STRUCTURES BEHIND PLUNGING
AIRFOILS: A COMPARISON OF
NUMERICAL AND EXPERIMENTAL RESULTS**

K.D.Jones, C.M.Dohring and M.F.Platzer
Naval Postgraduate School
Monterey, CA

**34th Aerospace Sciences
Meeting & Exhibit**
January 15-18, 1996 / Reno, NV

WAKE STRUCTURES BEHIND PLUNGING AIRFOILS: A COMPARISON OF NUMERICAL AND EXPERIMENTAL RESULTS

K. D. Jones[†], C. M. Dohring[‡] and M. F. Platzer*

Department of Aeronautics and Astronautics
Naval Postgraduate School
Monterey, California

Abstract

Comparisons are made between numerically and experimentally produced wake structures behind airfoils undergoing rapid, oscillatory plunging motions. Numerical simulations are performed using an unsteady panel code. Inviscid, incompressible flows about arbitrary moving airfoils are computed with the unsteady wake approximated by discrete point vortices, tracked using a Lagrangian mesh scheme. Numerically computed results are visualized using an interactive, graphical-animation interface. Experimental data are obtained from a low-speed water tunnel. Two-color dye injection is used to visualize unsteady wake structures, and velocity data are acquired using laser doppler velocimetry. Comparisons of vortex location agree well with linear theory for low amplitude motions. For large amplitude, high frequency motions, results diverge from linear theory, but wakes from the two approaches compare well with each other, including highly non-linear, non-symmetric wakes obtained for high amplitude, high frequency motions. Computed velocity profiles and integrated thrust coefficients for both approaches agree well.

Nomenclature

c = chord length
 C_d = drag coefficient per unit span, $D/(q_\infty c)$
 C_l = lift coefficient per unit span, $L/(q_\infty c)$
 C_t = thrust coefficient per unit span, $T/(q_\infty c)$
 D = drag per unit span
 h = plunge amplitude in terms of c
 k = reduced frequency, $\omega c/V_\infty$

L = lift per unit span
 q_∞ = freestream dynamic pressure $\frac{1}{2}\rho_\infty V_\infty^2$
 t = time
 T = thrust per unit span ($T = -D$)
 V_p = nondimensional plunge velocity, hk
 V_∞ = freestream velocity
 α = angle of attack
 λ = wake wavelength in terms of c
 ω = circular frequency
 ρ_∞ = freestream density
 τ = nondimensional time, tV_∞/c

Introduction

It is well known that the wake generated by an airfoil moving in a fluid may strongly influence the motion of a second airfoil. Indeed, wake interference can prevent or cause flow separation, it can suppress or promote aeroelastic flutter, and it can increase or decrease flight performance. Experience has shown that failing to consider wake interference effects can ultimately lead to disaster. On the other hand, proper use of wake interference can significantly boost overall performance, as is the case with insect flight.

In recent years an unsteady panel code for single and two-foil systems has been developed for the systematic study of flutter and wake interference.^{1,2} Numerically, if the wake/airfoil interaction is to be computed with any success, it is vitally important that the interfering wake be accurately represented. In reality the wake behind a moving airfoil contains a continuous distribution of vorticity, instantaneously equal in magnitude and opposite in orientation to the change in circulation about the moving airfoil. The unsteady panel code models the wake by releasing a discrete vortex at each time step equal in magnitude and opposite in direction to the change in circulation about the airfoil from the previous time step. After release the vortex is convected downstream, influencing and being influenced by the airfoil and the other discrete

[†] NRC Research Associate, Member, AIAA

[‡] Graduate Student, LCDR German Navy

* Professor, Associate Fellow, AIAA

This paper is declared a work of the U.S. Government and is not subject to copyright protection in the United States.

wake vortices. In order to enable visualization of the unsteady wake formation and evolution an interactive graphics animation interface is used.

In past studies (Refs. 3-6) results from the panel code have been compared to the theoretical studies of Theodorsen and Garrick,⁷ Smilg⁸ and Loewy,⁹ with good success. However, these theoretical studies applied linear theory to evaluate infinitely thin airfoils undergoing infinitesimal motions, providing little confidence in the accuracy of the panel code for thicker airfoils and larger amplitude displacements. Tuncer et al.¹⁰ found a good comparison between the wake patterns produced by the potential-flow code and vorticity data computed by a Navier-Stokes code for plunging motions.

To further validate the unsteady panel code and to aid in defining its limits of applicability, the unsteady wake structures numerically generated are compared to the wake structures found experimentally. In the past the wake patterns behind airfoils undergoing small amplitude pitching oscillations were experimentally investigated by Koochesfahani.¹¹ Wakes behind plunging airfoils were experimentally and numerically investigated by Bratt¹² with additional numerical comparisons made by Katz and Weihs.¹³ Experimental studies of Freymuth¹⁴ for airfoils plunging sinusoidally demonstrated thrust production. This was also demonstrated experimentally by Triantafyllou et al.¹⁵ with regard to fish propulsion, and they noted that it was possible to produce drag or thrust depending on the Strouhal number. Flapping wing propulsion was demonstrated numerically by Platzer et al.³ with an earlier version of the panel code used in the present study. For the present experimental work airfoils are plunged sinusoidally in a low-speed water tunnel, and both flow visualization and laser doppler velocimeter (LDV) data are obtained.

In this paper the numerical methods used in the panel code are outlined, the applied experimental techniques are detailed, and a direct comparison of results is presented.

Methods

The numerical and experimental methods utilized are detailed in the following subsections.

Numerical The production of the numerical wake data involves two key components; an unsteady flow solver and an interactive graphics animation interface. Flow solving is performed with an unsteady potential-

flow code developed at the Naval Postgraduate School by Teng.¹ The panel code computes inviscid, incompressible flows about arbitrary airfoils performing defined pitching or plunging motions. The code follows closely the original method of Hess and Smith,¹⁶ while with regard to the modeling of the unsteady wake it adopts the procedure of Basu and Hancock.¹⁷

Uniform source and vorticity distributions are placed on each panel at time t . The wake consists of a single vorticity panel attached as an additional element on the airfoil through which discrete vortices are shed into the wake and convected downstream with the fluid. A uniform vorticity distribution is placed on the wake panel, and it is further characterized by its length and inclination with respect to the local frame of reference. After each time step, the vorticity of the wake panel is concentrated into a single point vortex and convected downstream. Simultaneously, a new wake panel is formed.

The flow tangency conditions are satisfied at the exterior mid-points (control points) of each panel. The Kutta condition postulates that the pressure on the upper and lower surface at the trailing edge be equal. The wake panel is formed with a length and inclination to the local frame of reference that satisfies the Helmholtz theorem;

$$\Delta_k(\gamma_w)_k + \Gamma_k = \Gamma_{k-1} . \quad (1)$$

Equation (1) introduces an additional boundary condition, the conservation of vorticity. However, the introduction of the wake creates three additional unknowns; the vorticity of the wake panel, its length and its inclination. Therefore, two additional conditions are required:

1. The wake panel is oriented in the direction of the local resultant velocity at the panel midpoint.
2. The length of the wake panel is proportional to the magnitude of the local resultant velocity at the panel midpoint and the size of the time step.

The essential elements of this scheme are summarized in Fig. 1. Note, implementation of this approach requires an iterative scheme. The velocity direction and magnitude at the wake panel midpoint are not initially known and must be iteratively determined.

Details of the algorithm are given in Ref. 1, and the code is evaluated through comparisons with theoretical studies and Navier-Stokes simulations in Refs. 3-6 and 10.

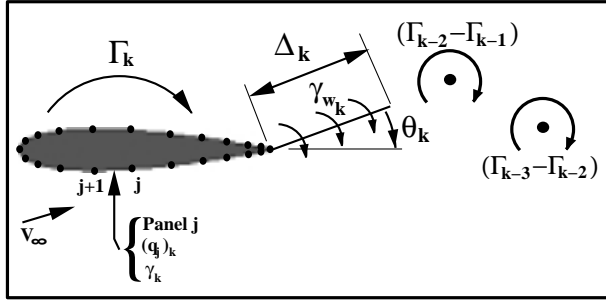


Fig. 1. Schematic of the panel code wake model.

To visualize the unsteady formation and evolution of the wake, an interactive graphics animation interface was developed. Details of the interface are found in Ref. 18 with a brief summary given here.

The animation package may be run concurrently with the potential-flow code, displaying the airfoil position and its wake, as well as the instantaneous surface pressure and time histories of the position variables and lift, drag and moment coefficients. Although the panel code is relatively efficient, it cannot compute a solution real-time, in fact, each time-step requires slightly more time to compute than the previous step. Therefore, an option is included to save the necessary data needed to regenerate the animation sequence in a compact, binary format, such that it may be replayed at a later time. The replay utility provides VCR-like controls, with pause, single-step forward/reverse and fast-forward/rewind options, reanimating the sequence at a smoother, more fluent frame-rate.

The graphics interface provides the user with many controls for the display format. For example, the wake is computed using a Lagrangian mesh scheme, with grid points attached to the individual vortex cores. Visualizing the wake by merely connecting the wake points in the order they were generated may result in a very confused representation of the wake. Discrete vortices may roll up into larger eddies, which may in turn be split by other large eddies. Often discrete vortices of opposite rotational direction and similar magnitude break away from the rest of the wake and travel through the flow as a vortex doublet. Although simply connecting the vortices with a line colored by the local vorticity magnitude is an available option, several other wake representations are provided.

To further enhance the *virtual wind tunnel* feel of the code, several additional tools are provided for probing and visualizing the flow, including a particle trace utility to simulate smoke rakes or dye injection, and a velocity profiler to simulate LDV results.

To facilitate measurement of vortex size and location, a grid may be overlaid on the wake image, with cell dimensions equal to the airfoil chord length. For cases with very small scale wake structures, a finer grid may be used. Still pictures are made by pausing the animation at a desired frame and using a *snapshot* or screen-dump utility to digitally record the image displayed on the screen. Data is presented in a nondimensional form, with lengths scaled by c , velocity scaled by V_∞ and time scaled by c/V_∞ .

Experimental The experiments were carried out in the Naval Postgraduate School water tunnel facility (Fig. 2). This is a closed circuit, continuous flow facility with a contraction ratio of 6:1 and horizontal orientation. The test section is 38cm wide, 51cm high and 150cm long. Glass side and bottom walls permit maximum optical access. There is no sealed cover, thus providing simple access to the model. The side walls of the test section diverge slightly to compensate for boundary layer growth and to maintain uniform flow velocity.

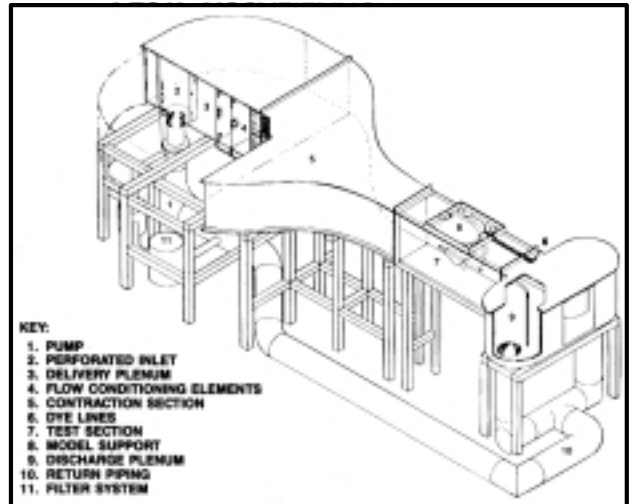


Fig. 2. Schematic of the NPS water tunnel.

The flow velocity can be set in a range from 0 to 0.5 m/s. It is measured by a flow meter at the end of the test section and digitally displayed. The freestream flow velocity in the test-section at the airfoil location is measured by LDV without the airfoil installed. The Reynolds number based on the airfoil chord length ranges between 500 for the smallest airfoil at low velocities up to 100,000 for the largest airfoil at high flow velocities.

For flow visualization water soluble food coloring is used. The dye is injected above and below the

airfoil by two individually routed lines with adjustable horizontal and vertical position. Some experiments were carried out with only one injector upstream of the airfoil, also yielding clear wake signatures. Pressurization for the dye canisters is provided by a small compressor.

The flow visualization experiments are conducted with a 1cm chord length airfoil similar to a NACA 0012. For the LDV measurements a NACA 0012 airfoil with a chord length of 10cm and an airfoil resembling a NACA 0015 with a 2cm chord length are also used. All airfoils have a wing span of 37cm and stretch across the whole test section. The airfoils are attached to a vertical shaker which is mounted on top of the test section. The frequency can be adjusted continuously from 5Hz to 60Hz. The amplitude can be adjusted from 0 to a maximum value which depends on the frequency. The amplitude is determined from the writing of a fixed position needle on a paper which is attached to the moving part of the shaker.

Most measurements are conducted with a constant frequency of 5Hz or 10Hz, changing the reduced frequency by adjusting the flow velocity in the tunnel. Measurements are done both at fixed reduced frequency/variable amplitude and fixed amplitude/variable reduced frequency. The wake patterns are photographed with a 35mm camera and the vortical wavelength is measured from the photographs using a ruler with appropriate scale. The vortical wavelength is defined as the distance between adjacent vortices of the same rotational direction, as shown in Fig. 3, and it is taken here as the average of the first three fully developed vortex pairs.

The LDV measurements are performed with a dual beam frequency shifted 300 mW Argon Ion laser with a beam separation of 50mm, a focal length of 350mm and back scatter receiving optics. The TSI FIND software is used. The vertical distribution of the mean streamwise velocity component is measured upstream and downstream of both the stationary and the plunging airfoil. The sample size is between 400 and 1000 at an average data rate between 5 and 20Hz; thus, a velocity averaged over several cycles is obtained.

Results

The presentation of results is divided into two general sections; comparisons of wake structures (flow visualization) and comparisons of velocity profiles and integrated thrust coefficients (LDV). First we must clarify use of the term *wake*. In reference to the vortex

street generated by an oscillating airfoil, *wake* refers to the vortical structures, implying nothing about the net drag on the airfoil. In reference to velocity profiles downstream of the airfoil, the term *wake* implies a net drag on the airfoil whereas *jet* indicates a net thrust.

Flow Visualization In viscous fluids, stationary airfoils and airfoils plunging sinusoidally with low V_p generate drag. As the V_p is increased the drag is reduced and eventually thrust is produced. The vortex streets indicative of drag, neutral and thrust producing cases are shown schematically and experimentally in Figs. 3,4 and 5, respectively. Experimental results for the three cases are for the 1cm airfoil oscillating at $k = 3.6$ and $h = 0.08$ ($V_p = 0.29$), $k = 4.7$ and $h = 0.12$ ($V_p = 0.56$) and $k = 3.0$ and $h = 0.20$ ($V_p = 0.60$), respectively.

Comparing Figs. 3 and 5 it should be noted that the upper row of vortices in Fig. 3 have a clockwise rotation, indicating drag production, whereas, in Fig. 5 they have a counter clockwise rotation, indicative of thrust production.

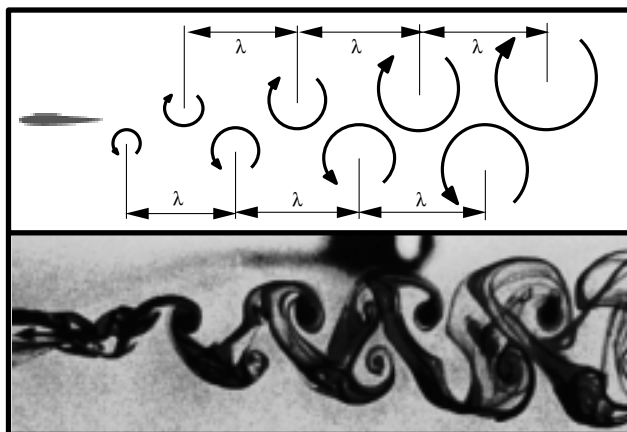


Fig. 3. Vortex street indicative of drag.

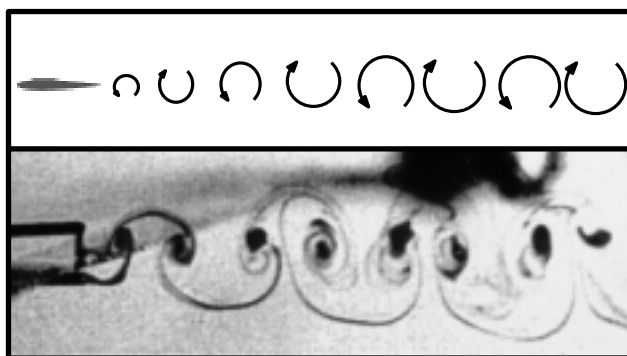


Fig. 4. Vortex street indicative of zero drag.

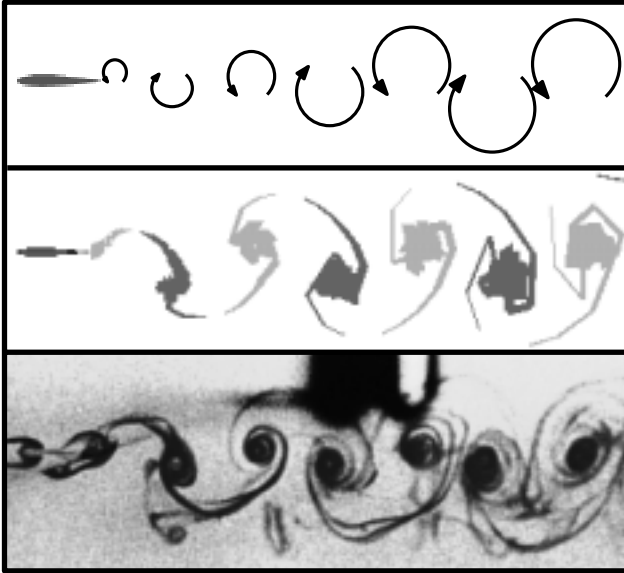


Fig. 5. Vortex street indicative of thrust.

For large V_p it is possible to generate a *dual-mode* or nonsymmetric vortex street, as shown in Fig. 6.

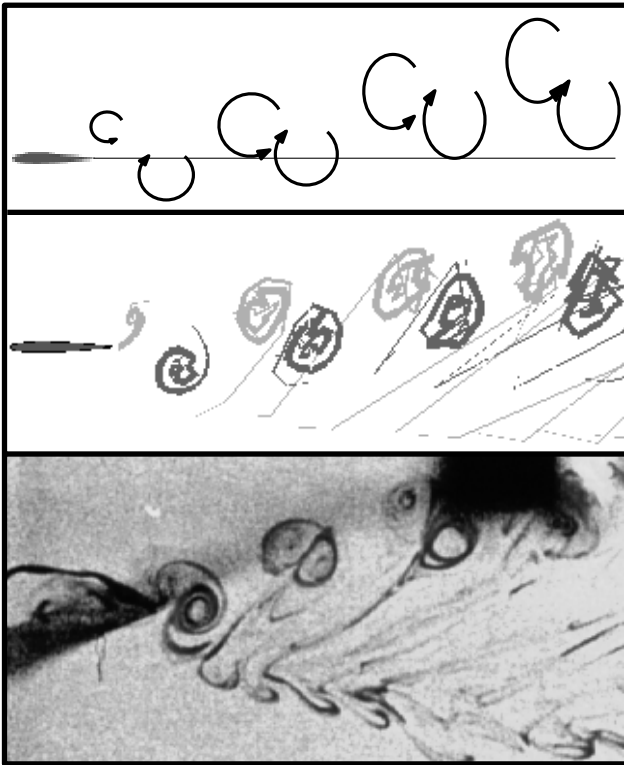


Fig. 6. Vortex street indicative of thrust/lift.

In this case $k = 10.1$ and $h = 0.20$ resulting in $V_p = 2.2$. Here in addition to a net thrust, a net lift

is observed according to the deflection of the vortex street.

In these figures the upper image is a schematic illustrating the rotational orientation of the eddies, and the lower image is a photo from the water tunnel. In Figs. 5 and 6, the central image is a snapshot of the wake structures computed by the panel code. The potential-flow code predicts zero drag for a stationary airfoil and thrust for an airfoil plunging at any frequency. Consequently, there are no numerical solutions with wake structures comparable to those in Figs. 3 and 4.

Deflected vortex streets of this nature were observed experimentally by Bratt, although no explanation or discussion regarding the phenomenon was given.

Numerically, the mode (vortex-street deflected up or down) is determined by the initial conditions, and appears to be fixed throughout the simulation. However, in the water tunnel the vortex street may alternate between modes somewhat randomly suggesting that relatively small disturbances may trigger the switch. This is discussed more in the next section.

Qualitative and quantitative comparisons of the wake structures are made by comparing photographs of the water tunnel experiments with the digital images from the panel code, such as those shown in Figs. 5 and 6. The measured wake wavelengths are plotted in Fig. 7 as a function of the plunge amplitude, for $k = 3.00$, $k = 6.83$ and $k = 12.32$. In all three cases, the curves from the panel code linearly extrapolate to the wavelengths predicted by linear theory ($\lambda = 2\pi/k$); $\lambda = 2.09$, $\lambda = 0.92$ and $\lambda = 0.51$, respectively.

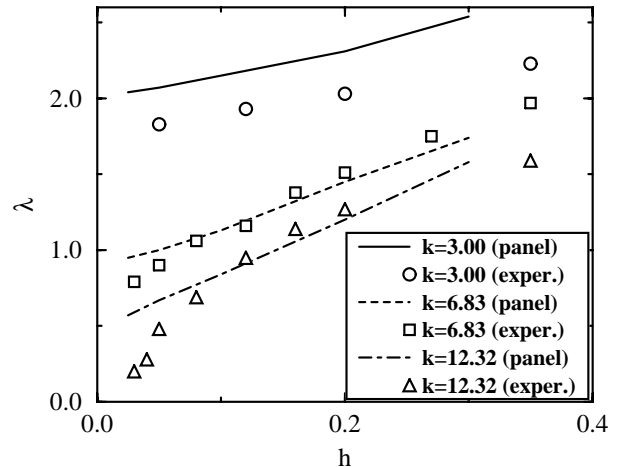


Fig. 7. Wake wavelength versus plunge amplitude.

The panel code predicts a thrust that is proportional to the square of V_p . For all non-zero V_p the panel code predicts a positive thrust and, hence, a wake wavelength larger than that predicted by linear theory. In Fig. 8 the wake wavelength is plotted as a function of k . Note that the panel-code results approach linear theory as hk approaches zero. However, the agreement between experiment and the panel code is better as hk increases, and for small hk the experimentally measured wavelengths are shorter than that predicted by linear theory, i.e., drag, not thrust, is produced. This is verified by the experimental wake pattern shown in Fig. 3 which resembles the characteristic drag-producing Karman vortex street generated by a cylinder in viscous flow.

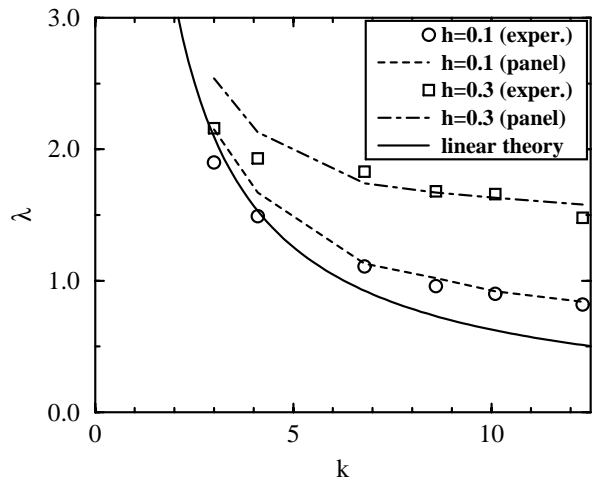


Fig. 8. Wake wavelength versus reduced frequency.

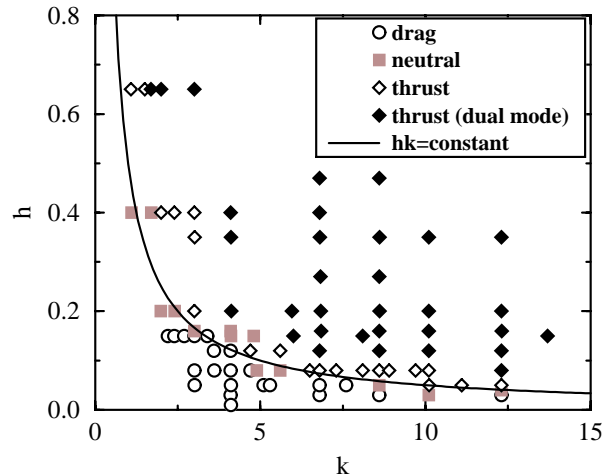


Fig. 9. Drag/thrust as a function of h and k .

According to the positions of vortices with clockwise and counter clockwise rotations (as illustrated in Figs. 3-6) the experimental results are classified in Fig. 9 as drag producing, neutral, thrust producing, and dual-mode thrust producing. A line of constant V_p is included demonstrating the dependence on V_p . This dependence on V_p was pointed out by Triantafyllou et al., although they apparently did not observe the dual-mode behavior shown here. Note, V_p is a nondimensional term that is roughly equivalent to the Strouhal number, using the plunge amplitude as the length scale, i.e., $V_p = \omega h / V_\infty$.

LDV Measurements Integrated lift, moment and drag results are output from the potential-flow code, and the thrust coefficient is computed by averaging the negative of the drag coefficient over a cycle. In the water tunnel, velocity profiles are measured in the wake by LDV, and from velocity data the thrust is computed using the equation;

$$T = \rho_\infty \int_{-\infty}^{+\infty} V(y)(V(y) - V_\infty) dy. \quad (2)$$

Nondimensional velocity profiles computed by the panel code and measured in the water tunnel are compared in Figs. 10, 11 and 12, for cases with $k = 4$ and $h = 0.088$ ($V_p = 0.35$), $k = 15$ and $h = 0.04$ ($V_p = 0.60$) and $k = 26$ and $h = 0.088$ ($V_p = 2.29$), respectively. In Figs. 10 and 12 the profile is measured $0.75c$ downstream of the trailing edge of the 2cm NACA 0015 airfoil oscillating at 10Hz with freestream velocities of $0.300m/s$ and $0.048m/s$, respectively.

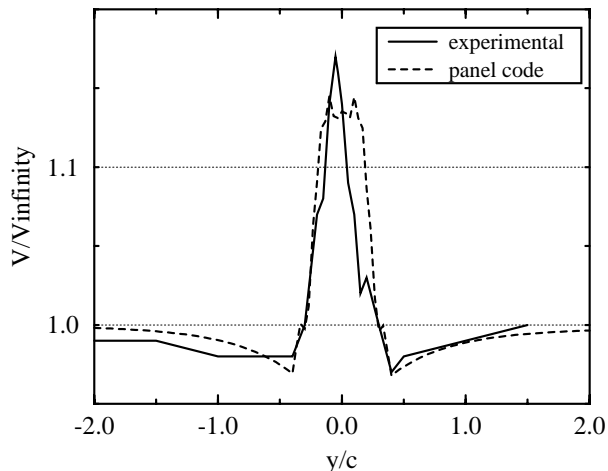


Fig. 10. Velocity profile comparison, $V_p = 0.35$.

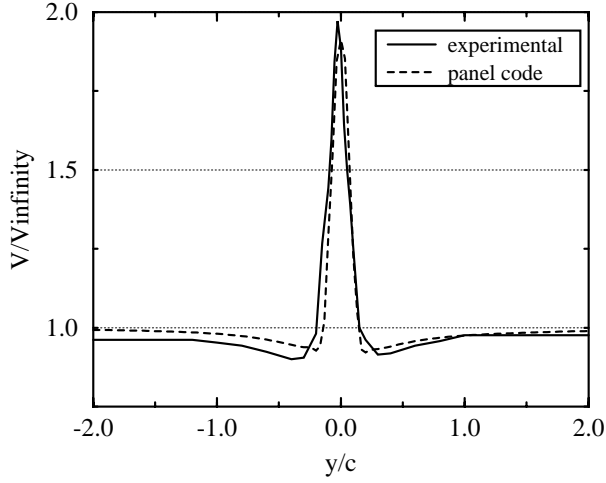


Fig. 11. Velocity profile comparison, $V_p = 0.60$.

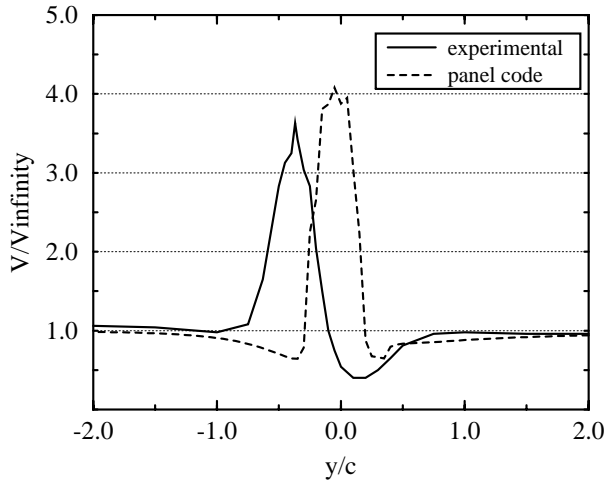


Fig. 12. Velocity profile comparison, $V_p = 2.29$.

In Fig. 11 the profile is measured $0.4c$ downstream of the trailing edge of the 10cm NACA 0012 oscillating at 5Hz with a freestream velocity of $0.210m/s$. Note, the accuracy of the experimental oscillation amplitudes is $\pm 0.25mm$, thus the amplitude error for the 2cm airfoil tests is considerably larger than for the 10cm airfoil.

The agreement between computational and experimental velocity profiles is quite good for the lower values of V_p . As V_p increases the experimentally measured profiles exhibit a highly nonsymmetric profile with a strong thrust peak on the side that the vortex street is deflected and a pronounced wake peak on the opposite side, as seen in Fig. 12. The cause of this asymmetric profile is not clear from the flow visualiza-

tion data, but a logical explanation is that it is due to massive separation on the suction side of the airfoil, i.e., the side opposite the deflected vortex street. Some asymmetry is found in the numerical velocity profiles, but to a much lesser degree. This is consistent with the above theory, as the panel code can only model attached flows.

Integrating the velocity profiles using Eq. (2) the thrust coefficients are computed, and these are compared to the numerical results in Figs. 13a and 13b as a function of k . Three numerical curves are plotted corresponding to the experimental error range in plunge amplitude, and three experimental curves are included corresponding to the experimental error range in the measured velocities.

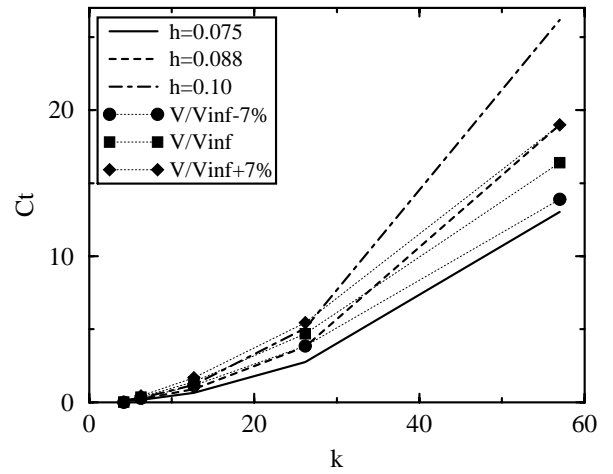


Fig. 13a. Thrust dependence on k .

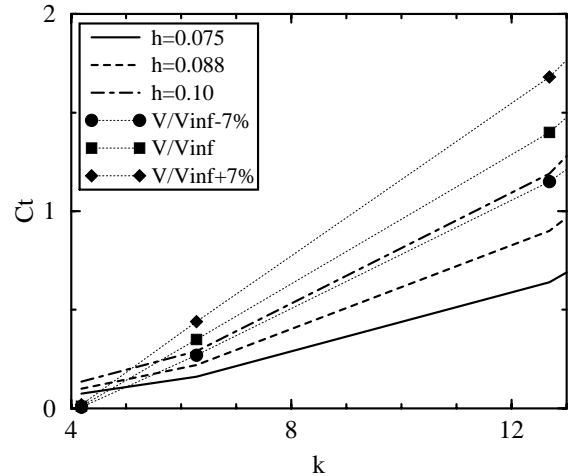


Fig. 13b. Thrust dependence on k (low k detail).

Note that the numerical thrust coefficient curves asymptotically approach zero as k approaches zero, in direct accordance with linear theory. In the detailed view of the low frequency range shown in Fig. 13b, experimentally it can be seen that for k less than about 4, drag not thrust will be produced. Also, at high frequencies the experimental results again fall below the predictions of the panel code, which agrees with the proposed theory of flow separation.

It was previously mentioned that the experimental wake patterns may alternate randomly between modes (vortex street deflected up or down). This can be seen clearly in the LDV measurements. In Fig. 14 the LDV data for two passes through the flowfield of the 1cm airfoil is shown, and both modes are apparent. The numbered points on the two curves indicate the order in which the velocity samples were taken, and it can be seen that the wake switched mode twice during the experiment.

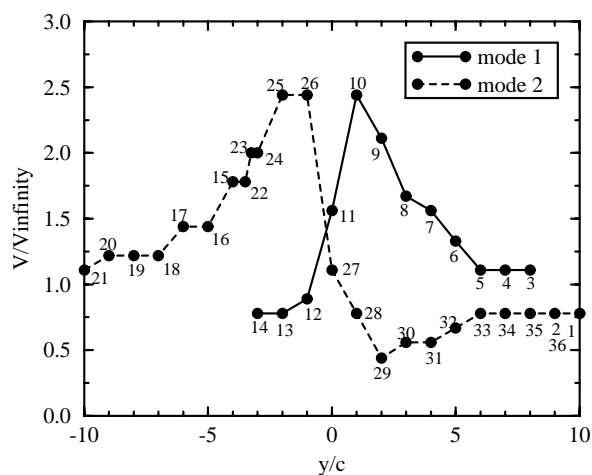


Fig. 14. Dual-mode LDV measurement.

Conclusions

Numerical methods were described for computing unsteady flowfields about oscillatory plunging airfoils and for graphically animating the motion of the airfoil and the associated wake. Experimental techniques were detailed for the generation and measurement of the same flowfields in a water tunnel, using two-color dye injection to illuminate the vortical structures and laser velocimetry to measure the wake/thrust velocity profiles and estimate the thrust generated by the foil's motion. Qualitative and quantitative comparisons were made of the wake geometry and the time-averaged thrust.

Presented flow visualization results indicate excellent agreement in the computed and measured wake geometries. Agreement deteriorates at lower plunge velocities, where viscous effects dominate inertial effects. A dual mode wake structure is found in both approaches, with non-symmetric wake structures that yield an average thrust and lift on the airfoil.

Experimental LDV data agree well with the numerical predictions over a wide range of oscillation frequencies and plunge amplitudes indicating that the development and evolution of the vortex street over a wide range of plunge velocities is governed primarily by inviscid flow effects. At low plunge velocities viscous effects become dominant and drag rather than thrust is measured in the water tunnel. Also at high plunge velocities, flow features not predicted by the panel code, such as flow separation, start to dominate the flow.

Acknowledgements

This investigation was partially supported by the Naval Postgraduate School National Research Council Fellowship Program (KDJ) and the Office of Naval Research (MFP), project officer Dr. P. Majumdar..

References

- ¹ Teng, N. H., "The Development of a Computer Code for the Numerical Solution of Unsteady, Inviscid and Incompressible Flow over an Airfoil," Master's Thesis, Naval Postgraduate School, Monterey, CA, June 1987.
- ² Pang, C. K., "A Computer Code for Unsteady Incompressible Flow past Two Airfoils," Aeronautical Engineer's Thesis, Naval Postgraduate School, Monterey, CA, Sept. 1988.
- ³ Platzer, M. F., Neace, K. S. and Pang, C. K., "Aerodynamic Analysis of Flapping Wing Propulsion," AIAA Paper No. 93-0484, Jan. 1993.
- ⁴ Riester, P. J., "A Computational and Experimental Investigation of Incompressible Oscillatory Airfoil Flow and Flutter Problems," Master's Thesis, Naval Postgraduate School, Monterey, CA, June 1993.
- ⁵ Turner, M., "A Computational Investigation of Wake-Induced Airfoil Flutter in Incompressible Flow and Active Flutter Control," Master's Thesis, Naval Postgraduate School, Monterey, CA, March, 1994.

- ⁶ Jones, K. D. and Platzer, M. F., "Time-Domain Aeroelastic Analysis of a two Airfoil System with Application to Unsteady Rotary Wing Flowfields," AIAA Paper No. 95-0337, Jan., 1995.
- ⁷ Theodorsen, T. and Garrick, I. E., "Mechanism of Flutter," NACA TR-685, 1940.
- ⁸ Smilg, B., "The Instability of Pitching Oscillations of an Airfoil in Subsonic Incompressible Potential Flow," **Journal of the Aeronautical Sciences**, Vol. 16, No. 11, Nov. 1949, pp. 691-696.
- ⁹ Loewy, R. G., "A Two-Dimensional Approximation to the Unsteady Aerodynamics of Rotary Wings," **Journal of the Aeronautical Sciences**, Vol. 24, No. 2, Feb. 1957, pp. 81-106.
- ¹⁰ Tuncer, I. H., Platzer, M. F. and Ekaterinaris, J. A., "Computational Analysis of Flapping Airfoil Aerodynamics," Proc. ASME Fluids Engineering Division, FED-Vol. 196, June, 1994, pp. 9-18.
- ¹¹ Koochesfahani, M. M., "Vortical Patterns in the Wake of an Oscillating Airfoil," **AIAA Journal**, Vol. 27, No. 9, Sept. 1989.
- ¹² Bratt, J. B., "Flow Patterns in the Wake of an Oscillating Airfoil," Aeronautical Research Council, R&M 2773, 1953.
- ¹³ Katz, J. and Weihs, D., "Behavior of Vortex Wakes from Oscillating Airfoils," **Journal of Aircraft**, Vol. 15, No. 12, Dec. 1978, pp. 861-3.
- ¹⁴ Freymuth, P., "Propulsive Vortical Signatures of Plunging and Pitching Airfoils," **AIAA Journal**, Vol. 26, No. 7., 1988, pp. 881-883.
- ¹⁵ Triantafyllou, G. S., Triantafyllou, M. S. and Grosenbaugh, M. A., "Optimal Thrust Development in Oscillating Foils with Application to Fish Propulsion," **Journal of Fluids and Structures**, Vol. 7, No. 2, 1993, pp. 205-224.
- ¹⁶ Hess, J. L. and Smith, A. M. O., "Calculation of Potential Flow about Arbitrary Bodies," **Progress in Aeronautical Sciences**, Vol. 8, pp. 1-138, Pergamon Press, Oxford, 1966.
- ¹⁷ Basu, B. C. and Hancock, G. J., "The Unsteady Motion of a Two-Dimensional Aerofoil in Incompressible Inviscid Flow," **Journal of Fluid Mechanics**, Vol. 87, 1978, pp. 159-168.
- ¹⁸ Jones, K. D. and Center, K. B., "Numerical Wake Visualization for Airfoils Undergoing Forced and Aeroelastic Motions," AIAA Paper No. 96-0055, Jan., 1996.